

Influence of Surface Finish on the Dry Sliding Wear and Electrochemical Corrosion Behaviour of 316L Stainless Steel

Abhishek Chaudhary¹, Subrat Kumar Baral¹, Gaurav Tiwari¹, B. Ratna Sunil² and Ravikumar Dumpala^{1*}

¹Department of Mechanical Engineering, Visvesvaraya National Institute of Technology, Nagpur — 440010, India; ravikumardumpala@mec.vnit.ac.in

²Department of Mechanical Engineering, Bapatla Engineering College, Bapatla — 522101, India

Abstract

316L stainless steel is known for its high corrosion resistance and extensively being used for biomedical implants and for the fabrication of the parts in nuclear reactors, and fuel cells. In the current study, 316L stainless steel samples were grounded using different grades of surface grits (400, 1200, and mirror-finished) by mechanical polishing, and influence of surface finish on the wear and corrosion characteristics was studied. The dry sliding wear experiments were carried out on ball-on-plate setup against hardened steel ball and the corresponding friction curves were obtained and specific wear rates were measured. The wear mechanisms were identified by examining the worn-out surface using scanning electron microscope and Raman spectrometer. It was evident that the formation and removal of iron oxides is the dominant mechanism for material loss from the samples during wear tests. The higher wear resistance of the mirror-finished sample was attributed to the formation of stable chromium oxide layer on the wear track. Potentiodynamic polarization tests were performed on the samples and better corrosion resistance was observed for the mirror-finished sample.

Keywords: Electrochemical Corrosion, Raman Spectroscopy, 316L Stainless Steel, Sliding Wear, Surface Finish

1.0 Introduction

The 316L Stainless Steel (SS) has found applications in biomedical implants, Proton Exchange Membrane (PEM) of fuel cells, in-vessel components of the International Thermonuclear Experimental Reactor (ITER), automobile and aerospace industries¹⁻⁴. The components used in the above applications, especially in the automobile and aerospace industries required better wear resistance, whereas biomedical applications are subjected to highly corrosive body fluids⁵. High corrosion resistance of 316L SS is mainly accredited to presence of passive oxide layer on the surface, generated as a result of high amount of chromium in 316L SS⁶. It has been well established that

the corrosion performance of the metals mainly depends on temperature, humidity, pH of the medium, and surface roughness⁷⁻⁹. There have been studies that involve the use of surface roughness and its effect on corrosion resistance. The surface finish obtained in a specimen is a result of the manufacturing process used and the parameters used while manufacturing the component¹⁰.

Svahn *et al.* investigated the effect of surface finish on the tribological performance of tungsten and chromium coatings. It was reported that the rougher surface exhibits higher Coefficient Of Friction (COF) and there was a strong role of surface finish on frictional characteristics¹¹. Hanief *et al.* examined the influence of surface roughness on running wear behaviour of EN 31 steel. A model was

*Author for correspondence

developed representing the relation between the running wear behaviour and surface roughness. The model reported and validated by the experiment showed increase in the wear rate with higher surface roughness¹². Federici *et al.* reported the role of surface finish by conducting dry sliding wear tests on the samples coated using HVOF process. It was observed that the COF is increased with the increased surface finish¹³.

Abosrra *et al.* examined the role of surface finish on corrosion properties of mild steel and 316L SS. The 316L SS exhibited an increased corrosion rate with increased surface roughness¹⁴. Hady *et al.* reported the significance of surface finish on fretting corrosion of 316L SS. It was observed that fretting corrosion current increased with increase in surface roughness¹. Electropolishing (EP)¹⁵ and Magneto-Electropolishing (MEP)¹⁶ are processes that come under precision polishing operations. The EP processes influence the surface finish and lead to hydrophobic nature of the material surface¹⁵. The influence of magnetic field during electropolishing also produces variations in the surface finish and the MEP process was studied for its effect on corrosion resistance¹⁶. Lee *et al.* studied the effect of EP process and its influence on corrosion properties of 316L SS. It was reported that there was an improvement of 60-80 % in the uniform corrosion resistance in the 0.5M H₂SO₄ corrosion medium¹⁵. Hryniewicz *et al.* reported the role of MEP on corrosion resistance of medical grade 316L SS and compared the process with EP and Mechanical Polishing (MP). The results revealed that the MEP process produces the least uniform corrosion rate in all the tested media under the selected process parameters¹⁶. The process parameters used during Selective Laser Melting (SLM) also influences the surface finish of the component and hence the degradation rate. Ni *et al.* studied the role of inclination angle on surface finish and degradation rate of SLM treated 316L SS. It was reported that with the increase in surface roughness, corrosion current first increased and then decreased, which was attributed to the irregularities and inclusions during the process¹⁷.

The literature survey showed limited work on the role of surface finish on the electrochemical corrosion characteristics¹⁴ and no specific study on the wear behaviour. Hence in the current work, the effect of surface finish on the dry sliding wear and corrosion behaviour of 316L SS was investigated.

2.0 Experimental Details

The composition of 316L SS was analysed using spectroscopy analysis and presented in Table 1. For the microstructural study, the polished sample was etched using 50% concentrated Aqua regia for 60 seconds and observed under the optical microscope (Zeiss Axioskop 2 Mat, Germany). The X-ray diffractometer (Rigaku, Japan) was used for structural characterization using Cu-K α radiation and 2 θ angle from 30° to 90° with a scan rate of 2°/min. Microhardness of the samples was obtained using Vickers microhardness tester (Economet VH1-MDX, Chennai Metco, India) with a load of 100 g for 10 s dwell time.

For wear and corrosion tests, the 316L SS specimens of size 20mm×20mm were prepared using WEDM. The samples were polished starting with 100 grits to 400 grits, 1200 grits, and mirror finish to produce three samples of different surface roughness. The polished samples were cleaned using ethanol in ultrasonic cleaner before all the tests. Surface roughness of the samples was measured with the help of a 2D profilometer (Model: SJ410, Make: Mitutoyo, Japan). Figure 1(a) shows the schematic illustration of different surface roughness of three samples and Figure 1 (b, c, d) shows SEM micrographs of 400 grit, 1200 grit, and mirror-finished sample surfaces, respectively.

Dry sliding tribological test was performed on a reciprocating setup (TR-281, DUCOM). The counter body used was AISI 52100 hardened steel ball of 6 mm dia. The fixed ball was made to reciprocate against the substrate along a straight path with a constant load of 10 N, velocity of 0.06 m/s, and frequency of 5Hz with a total

Table 1. Chemical composition of as-received 316L SS

| Elements | Fe | Cr | Ni | Mo | Mn | Si | C | P | S |
|----------|--------|--------|--------|-------|------|-------|-------|-------|-------|
| Wt. % | 69.544 | 16.889 | 10.016 | 2.176 | 0.88 | 0.427 | 0.030 | 0.030 | 0.008 |

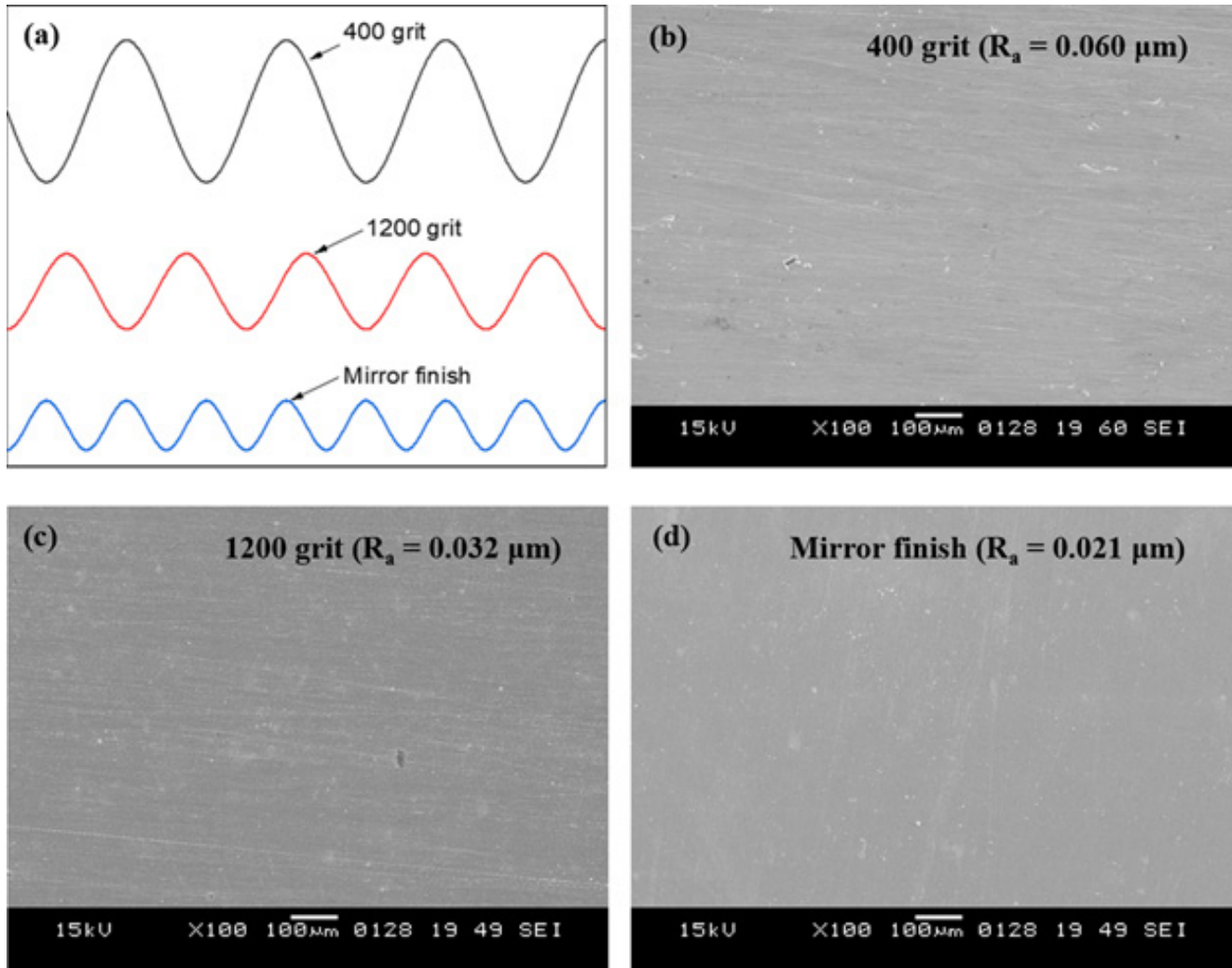


Figure 1. (a) Schematic of surface profile for different grades of surface finish. SEM micrographs of (b) 400 grits, (c) 1200 grits and (d) mirror-finished samples.

sliding distance of 100m. The load and frequency of the test were selected by keeping in mind the applications and conditions of the material during the actual use as well as the limitations of the tribometer. The loss in weight of the samples after wear tests was calculated and the corresponding specific wear rate was found using the below formula.

$$\text{Specific wear rate (mm}^3/\text{Nm)} = \frac{\text{Volume wear rate}}{\text{Total Sliding distance} \times \text{Load}}$$

Where, $\text{Volume wear rate (mm}^3) = \frac{\text{Mass loss}}{\text{Density}}$

The COF during the test was continuously recorded by the software and plotted against distance for each sample and the average COF for each sample was measured. The

worn-out surface characteristics were investigated using Scanning Electron Microscope (SEM) attached with Energy Dispersive X-Ray Spectrometer (EDS). Raman spectroscopy (NOST, South Korea) with a laser source of 532nm was also used to analyse the phases formed on the wear tracks.

The electrochemical corrosion test of 316L SS samples was performed using potentiodynamic polarization method by electrochemical analyser (CH Instruments, USA). The polarization tests were carried out using 3-electrode cell having an exposed area of 0.7854cm² for the working electrode. The working electrodes were the polished 316L SS samples having different surface finish. Graphite rod and Saturated Calomel Electrode (SCE) were utilised as the counter and reference electrodes,

respectively. The corrosion medium of 3.5% NaCl aqueous solution was prepared using NaCl and distilled water. At first Open Circuit Potential (OCP) test for 30 minutes was performed for stabilization, followed by the potentiodynamic polarization test. Tafel exploration test was performed for the scanning range of -700mV to 300mV using a scan rate of 1mV/s. The corrosion current (I_{corr}) and corrosion potential (E_{corr}) were calculated from the Tafel exploration plot. The corrosion rate in mm per year (mmpy) for the samples was measured using the following equation.

$$\text{Corrosion rate} = 0.00327 \frac{I_{corr}EW}{DA}$$

Where I_{corr} is the corrosion current (μA), EW is the effective weight of the specimen, D is density (g/cm^3), and A is the 3-electrode cell exposed area (cm^2).

For the 316L SS samples, a density of $7.99\text{g}/\text{cm}^3$ was used. The effective weight of the material is 27.9^{15} . The corrosion rate of the samples was calculated and compared.

3. Results and Discussion

3.1 Material Characterization

The optical microstructure and XRD plot of as-received 316L SS are shown in Figure 2(a) and (b), respectively. The microstructure of 316L SS revealed the austenite and ferrite phases as indicated by arrow. The γ -austenite can be seen in the microstructure as the light regions which was

confirmed by the XRD peaks having peaks (111), (200), and (220) as shown in Figure 2(b). Whereas, the dark-coloured grain boundary was confirmed as the δ -ferrite, which can be seen as a small branch and identified as peak (110) in the XRD. The Vickers microhardness of the material was measured as 164 ± 4.05 HV.

3.2 Friction and Wear Characteristics

The COF Vs. distance plot for all three samples is represented in Figure 3. It was apparent from the results that the COF decreased with improved surface finish. Rough surface (400 grit) exhibited the highest COF (0.64) and the mirror-finished surface showed the lowest COF (0.45) as presented in Table 2. Due to rough surface in case of 400 and 1200 grit samples, the counter body must overcome higher surface asperities during contact, thus higher frictional force and increased COF. In case of the mirror-finished sample, the surface is fine and smooth, thus lower friction force during the sliding of the counter ball on smooth surface, COF is lower. The running wear behaviour can also be differentiated clearly for the different surface roughness. In Figure 3, it is observed that the friction curve of the mirror-finished sample stabilised faster than the same of 400 grit and 1200 grit samples. In the beginning, due to contact with surface asperities, there is fluctuation in the COF curve but after some time, the curve is stabilized as a result of the formation of a stable tribo-oxide layer. It can be perceived from the COF plot that the mirror-finished sample stabilised after running

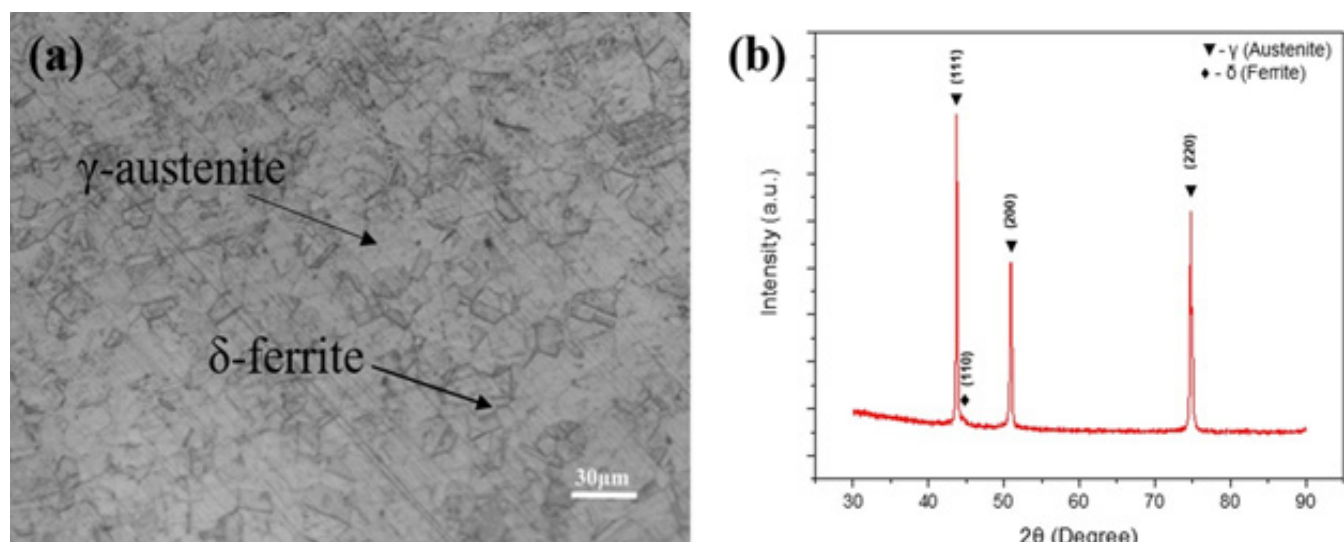


Figure 2. (a) Optical microstructure and (b) XRD pattern of 316L SS.

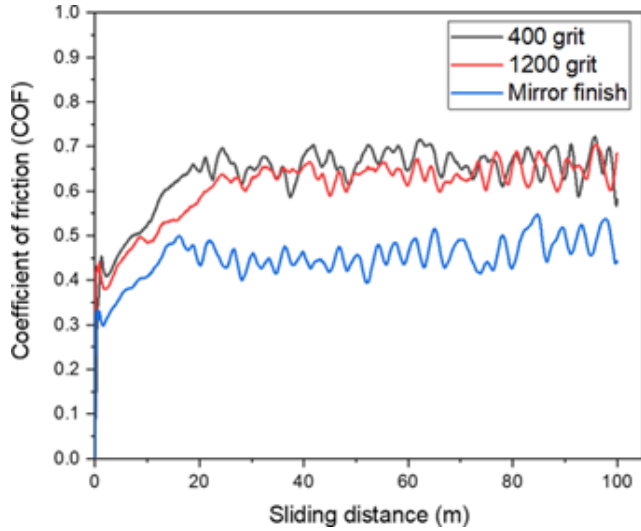


Figure 3. COF Vs. sliding distance plot for different polished samples.

15 m of sliding distance, which is faster in comparison to 400 grit and 1200 grit samples.

Figure 4 shows specific wear rate plot of all samples. It was observed that the wear rate decreased with decreased surface roughness. The continuous sliding of counter body results in the formation of oxide layers due to frictional heating and oxides were removed in the form of debris. In case of mirror-finished sample, this oxide layer is stable, thus lower debris is produced and specific wear rate is low as compared to 400 and 1200 grit sample. The 400 grit sample showed highest specific wear

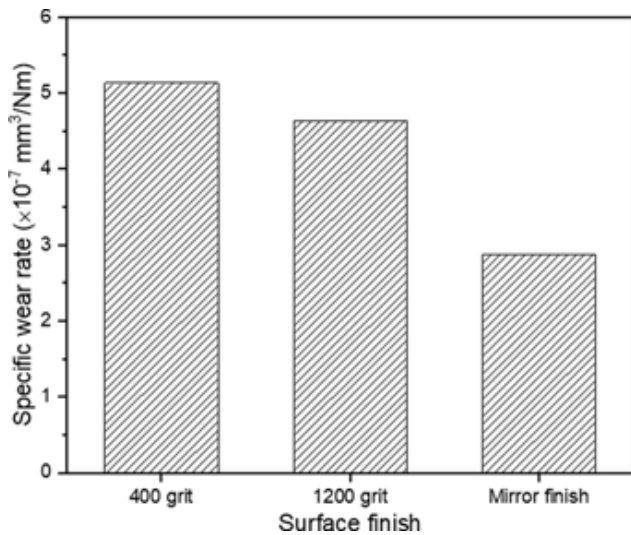


Figure 4. Specific wear rate of 400 grit, 1200 grit, and mirror-finished samples.

Table 2. Wear test results for different polished samples

| Sample | COF | Specific wear rate (mm^3/Nm) |
|---------------|------|--|
| 400 grit | 0.64 | 5.134×10^{-7} |
| 1200 grit | 0.61 | 4.6307×10^{-7} |
| Mirror finish | 0.45 | 2.8786×10^{-7} |

rate of $5.134 \times 10^{-7} \text{ mm}^3/\text{Nm}$, whereas the least wear rate of $2.8786 \times 10^{-7} \text{ mm}^3/\text{Nm}$ is observed by mirror-finished sample as shown in Table 2. It was observed that there is a 43% improvement in wear resistance for mirror-finished sample as compared to 400 grit sample.

Figure 5 shows worn-out SEM morphology of the sample surfaces. It was observed that width of wear track is increased with increase in surface roughness. Samples with high surface roughness resulted in larger contact widths as compared to the mirror-finished sample, which is attributed to the quick material removal through the asperity deformation and debris formation.

The Figure 5(a, b) shows the worn surface morphology of 400 grit sample in lower and higher magnification. Parallel grooves along the sliding direction and delaminated surface were visible. Abrasive action by hard asperities of counter body resulted in ploughing of material and formation of grooves. The substrate surface is oxidized due to frictional heating and oxide layers were formed but these layers are not stable and repeated sliding action removed the layers in the form of oxide debris, which is evident of oxidation wear. The repeated loading on the substrate surface led to generation of subsurface cracks from plastically deformed layer, which is propagated to the surface and results in to delamination wear. The Figure 5(c, d) shows presence of oxide debris and delaminated surface, thus oxidation and delamination are dominant wear mechanism in case of 1200 grit sample. Figure 5(e, f) shows smooth worn surface morphology with lower amount of debris and mild delamination. Due to better surface finish, the surface asperities are low and formation of stable oxide layers (Cr_2O_3) as observed from EDS and Raman spectroscopy are responsible for lower wear rate as well as lower COF.

The EDS analysis of 400 grit samples was shown in Figure 6, where the debris (white region, marked as Y) is iron oxide and the dark region is chromium oxide. The

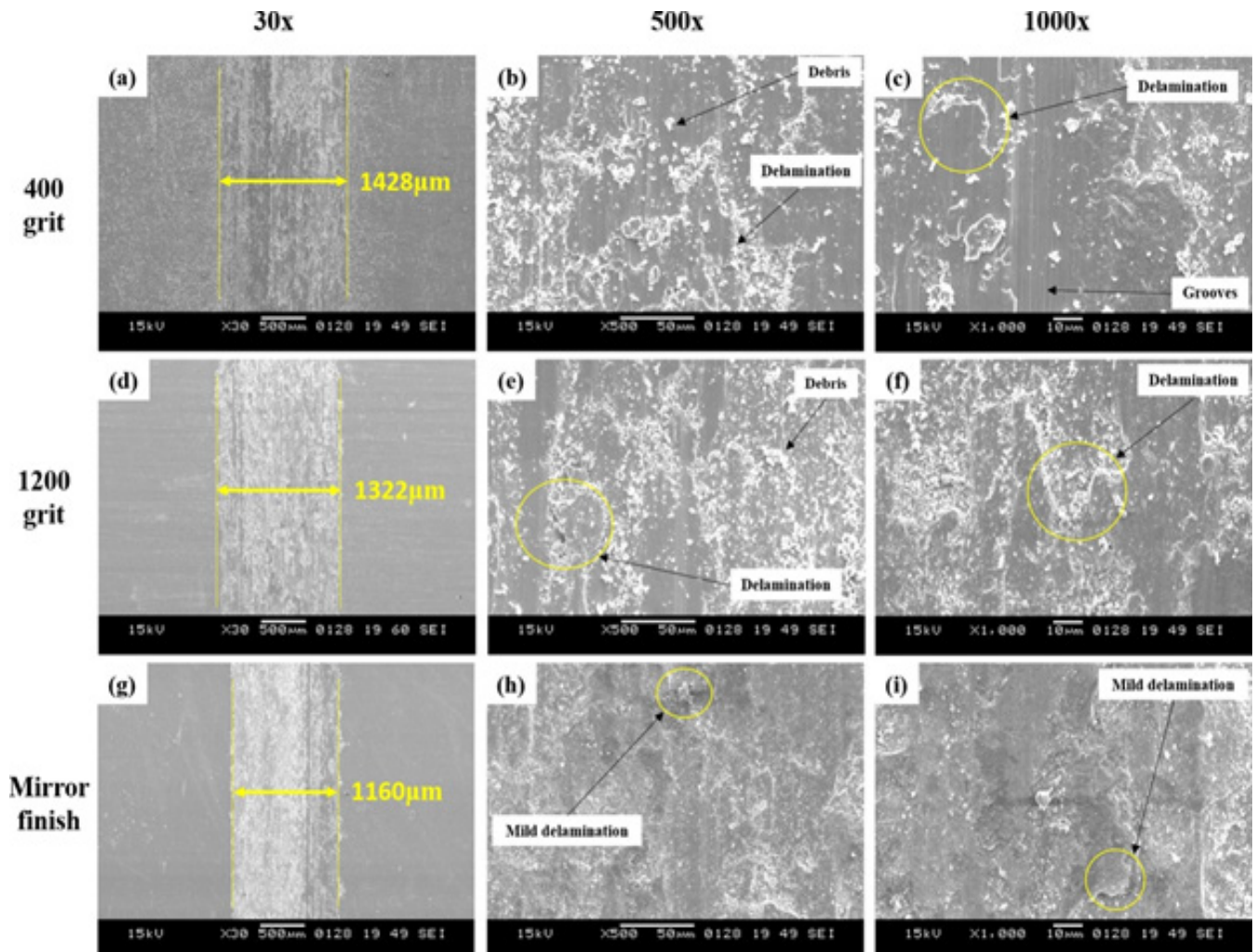


Figure 5. SEM images of worn surfaces for (a-c) 400 grit, (d-f) 1200 grit, and (g-i) mirror-finished samples.

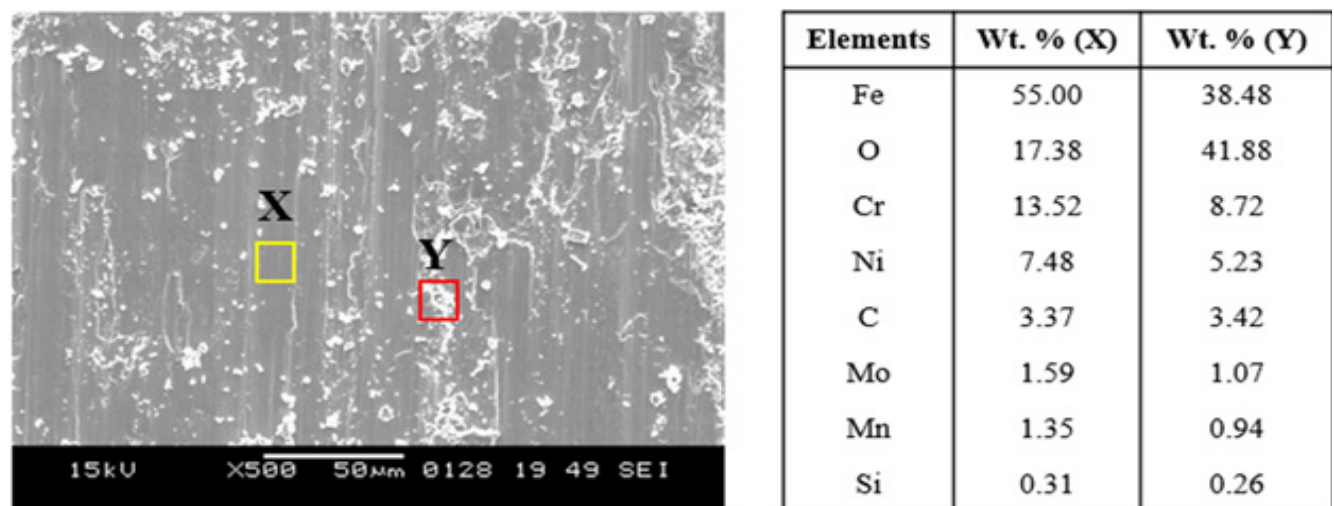


Figure 6. SEM micrograph and EDS analysis of worn surface of 400 grit samples.

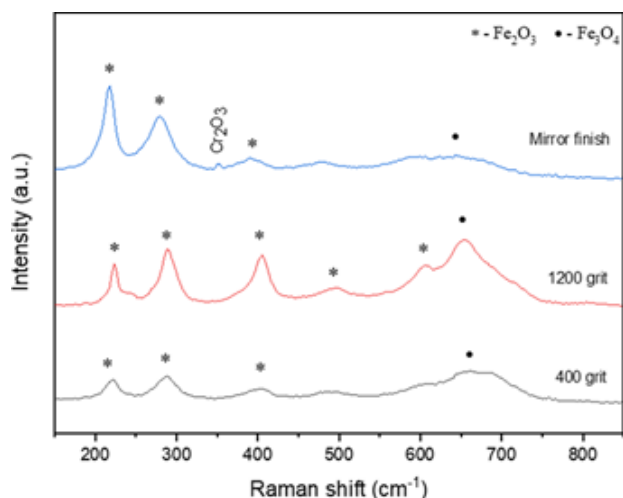


Figure 7. Raman spectra of worn surfaces of 400 grit, 1200 grit and mirror-finished samples.

presence of iron oxide increases the COF of the samples as stated by Godfrey¹⁸ and the presence of chromium oxide decreases the wear rate and stabilize the COF curve¹⁹.

The Raman spectroscopy of worn-out sample is shown in Figure 7. It was observed that iron oxides such as Fe_2O_3 and Fe_3O_4 was formed in all the samples, which is unstable and removed as oxide debris by continuous sliding action. Its removal increased the COF and wear rate. Whereas, the chromium oxide Cr_2O_3 as identified by the Raman spectroscopy in the mirror-finished sample is stable and attributed to improved wear resistance¹⁹.

3.3 Corrosion Study

Figure 8 shows Tafel plot of 400 grit, 1200 grit and mirror-finished samples were shown in the. The values of corrosion current (I_{corr}) and corrosion potential (E_{corr}) were measured from polarization plot using Tafel exploration method and is presented in the Table 3. The E_{corr} of 400 grit sample is higher (-0.193 V) than 1200 grit (-0.202

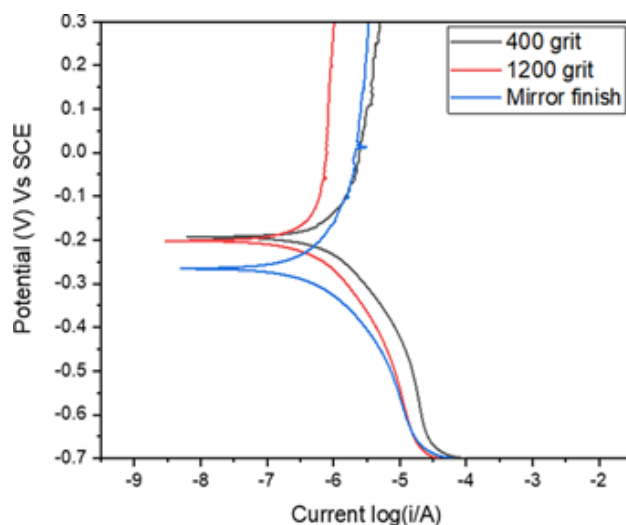


Figure 8. Tafel plot for the samples of 400 grit, 1200 grit and mirror polished in chloride solution.

V) and mirror-finished (-0.265 V) sample. The corrosion current decreased with increased surface finish, the 400 grit sample shows higher corrosion current of $2.54 \times 10^{-7} \text{ A/cm}^2$. Whereas, the corrosion current decreased for 1200 grit sample ($2.12 \times 10^{-7} \text{ A/cm}^2$) and further decreased for mirror-finished sample ($1.37 \times 10^{-7} \text{ A/cm}^2$). This suggests that the substrate is getting corrosion resistant with improved surface finish, since the charge transfer on the mirror-finished sample is 1.85 times higher than the 400 grit sample, which protects the surface from corrosion attack of chloride ions²⁰.

The I_{corr} was used to calculate the corrosion rate and presented in Table 3. The rougher surfaces exhibited higher I_{corr} values and hence attributed to higher corrosion rate. There was a decrease in corrosion rate of 16.53% in 1200 grit sample as compared to 400 grit samples and 46.06% decrease in corrosion rate from 400 grit sample to mirror-finished sample. It was observed that the surface finish has a significant effect on the corrosion rate of 316L SS.

Table 3. Results of potentiodynamic polarization test

| Sample | OCP (V) | E_{corr} (V) | i_{corr} (A/cm^2) | Corrosion rate (mmpy) |
|---------------|---------|-----------------------|---------------------------------------|-----------------------|
| 400 grit | -0.159 | -0.193 | 2.54×10^{-7} | 0.0029 |
| 1200 grit | -0.1162 | -0.202 | 2.12×10^{-7} | 0.0024 |
| Mirror finish | -0.1909 | -0.265 | 1.37×10^{-7} | 0.0015 |

Another reason for the change in corrosion rate can also be due to the fact that, as surface finish increases, better polishing of the surface takes place which in turn shows hydrophobic nature towards the corrosion medium. Because of that, the interaction between the surface and corrosion media is reduced which in turn decreases the corrosion rate.

4.0 Conclusion

- The sliding wear tests on 316L SS samples confirmed that the COF and wear rates were influenced by the surface finish of the sample. COF and specific wear rate increased with the increase in surface roughness. The 400 grit sample exhibited high COF and wear rate, whereas the mirror-finished sample exhibited low COF and wear rate.
- The continuous formation and removal of unstable iron oxides such as Fe_2O_3 and Fe_3O_4 are responsible for increased COF and wear rate. Whereas, stable chromium oxide Cr_2O_3 formed in mirror-finished sample is responsible for lower COF and wear rate.
- The potentiodynamic polarization tests confirmed the variations in corrosion rate with the surface finish. The corrosion rate decreased by 46.06% in the mirror-finished sample as compared to the 400-grit polished sample.

5.0 References

1. Hady H, Sabea Hammood A, Thair L. The role of surface roughness during fretting corrosion of 316L stainless steel. *Mater Today: Proc.* 2021; 42:2326-33. <https://doi.org/10.1016/j.matpr.2020.12.323>
2. Walczak J, Shahgaldi F, Heatley F. In vivo corrosion of 316L stainless-steel hip implants: morphology and elemental compositions of corrosion products. *Biomater.* 1998; 19(1):229-37. [https://doi.org/10.1016/S0142-9612\(97\)00208-1](https://doi.org/10.1016/S0142-9612(97)00208-1) PMID:9678872
3. Wang Y, Northwood DO. An investigation into TiN-coated 316L stainless steel as a bipolar plate material for PEM fuel cells. *J of Power Sources.* 2007; 165(1):293-8. <https://doi.org/10.1016/j.jpowsour.2006.12.034>
4. Zhong Y, Liu L, Wikman S, Cui D, Shen Z. Intragranular cellular segregation network structure strengthening 316L stainless steel prepared by selective laser melting. *J Nucl Mater.* 2016; 470:170-8. <https://doi.org/10.1016/j.jnucmat.2015.12.034>
5. Manivasagam G, Dhinasekaran D, Rajamanickam A. Biomedical implants: corrosion and its prevention - a review. 2010; 2:40-45. <https://doi.org/10.2174/1877610801002010040>
6. Talha M, Behera CK, Sinha OP. A review on nickel-free nitrogen containing austenitic stainless steels for biomedical applications. *Mater Scie and Eng: C.* 2013; 33(7):3563-75. <https://doi.org/10.1016/j.msec.2013.06.002> PMID:23910251
7. Guo L, Street SR, Mohammed-Ali HB, et al. The effect of relative humidity change on atmospheric pitting corrosion of stainless steel 304L. *Corros Sci.* 2019; 150:110-20. <https://doi.org/10.1016/j.corsci.2019.01.033>
8. Melchers RE. Effect of Temperature on the Marine Immersion Corrosion of Carbon Steels. *Corros.* 2002; 58(09):02090768. <https://doi.org/10.5006/1.3277660>
9. Wang Y, Cheng G, Wu W, Qiao Q, Li Y, Li X. Effect of pH and chloride on the micro-mechanism of pitting corrosion for high strength pipeline steel in aerated NaCl solutions. *Appl Sur Sci.* 2015; 349:746-56. <https://doi.org/10.1016/j.apsusc.2015.05.053>
10. Sultan AZ, Sharif S, Kurniawan D. Effect of Machining Parameters on Tool Wear and Hole Quality of AISI 316L Stainless Steel in Conventional Drilling. *Procedia Manuf.* 2015; 2:202-7. <https://doi.org/10.1016/j.promfg.2015.07.035>
11. Svahn F, Kassman-Rudolphi Å, Wallén E. The influence of surface roughness on friction and wear of machine element coatings. *Wear.* 2003; 254(11):1092-8. [https://doi.org/10.1016/S0043-1648\(03\)00341-7](https://doi.org/10.1016/S0043-1648(03)00341-7)
12. Hanief M, Wani MF. Effect of surface roughness on wear rate during running-in of En31-steel: Model and experimental validation. *Mater Lett.* 2016; 176:91-3. <https://doi.org/10.1016/j.matlet.2016.04.087>
13. Federici M, Menapace C, Moscatelli A, Gialanella S, Straffelini G. Effect of roughness on the wear behavior of HVOF coatings dry sliding against a friction material. *Wear.* 2016; 368-369:326-334 <https://doi.org/10.1016/j.wear.2016.10.013>
14. Abosrra L, Ashour A, Mitchell S, Youseffi MJCMPCP. Corrosion of mild steel and 316L austenitic stainless steel with different surface roughness in sodium chloride saline solutions. *WIT Transactions on Engineering Sciences.* 2009; 65:161-172. <https://doi.org/10.2495/ECOR090161>
15. Lee S-J, Lai J-J. The effects of electropolishing (EP) process parameters on corrosion resistance of 316L stainless

- steel. *J Mater Process Techn.* 2003; 140(1):206-10. [https://doi.org/10.1016/S0924-0136\(03\)00785-4](https://doi.org/10.1016/S0924-0136(03)00785-4)
16. Hryniewicz T, Rokicki R, Rokosz K. Corrosion Characteristics of Medical-Grade AISI Type 316L Stainless Steel Surface After Electropolishing in a Magnetic Field. *Corross.* 2008; 64(8):660-5. <https://doi.org/10.5006/1.3279927>
17. Ni C, Shi Y, Liu J. Effects of inclination angle on surface roughness and corrosion properties of selective laser melted 316L stainless steel. *Mater Res Express.* 2019; 6(3):036505. <https://doi.org/10.1088/2053-1591/aaf2d3>
18. Godfrey DJT, Technology L. Iron oxides and rust (hydrated iron oxides) in tribology. *Journal of the Society of Tribologists and Lubrication.* 1999; 55(2):33.
19. Cheng X, Jiang Z, Wei D, Wu H, Jiang L. Adhesion friction and wear analysis of a chromium oxide scale on a ferritic stainless steel. *Wear.* 2019; 426-427:1212-1221. <https://doi.org/10.1016/j.wear.2019.01.045>
20. Saldaña-Robles A, Plascencia-Mora H, Aguilera-Gómez E, Saldaña-Robles A, Marquez-Herrera A, Diosdado-De la Peña JA. Influence of ball-burnishing on roughness, hardness and corrosion resistance of AISI 1045 steel. *Surf and Coat Technol.* 2018; 339:191-8. <https://doi.org/10.1016/j.surfcoat.2018.02.013>